The Role of Tryptophan and Its Derivatives in Elucidating A PCET Mechanism in the Model Protein Azurin

Hanna LK Long

Department of Chemistry, East Carolina University, Greenville, NC 27858

April 2020

In partial fulfillment of the ECU Honors College Signature Honors Project under the supervision and guidance of Dr. Andrew Sargent

Abstract

The role and properties of electron-rich tyrosine in the proton-coupled electron transport (PCET) pathway has been extensively studied, specifically relating to ribonucleotide reductase.[1] Tryptophan is another electron-rich amino acid that can be derivatized into unnatural amino acids (UAAs) to further explore the mechanism of PCET.[2] The purpose of this study is to computationally study the properties of tryptophan and its derivatives, modeled as simplified indole rings, to rationalize key experimental findings. Calculations were performed using density functional theory (DFT) to provide information on structure, energetics, and properties in a reliable, efficient manner. Ionization potentials of the halogenated and hydroxylated indole rings were studied with and without a solvent environment to understand certain features of the experimentally derived Pourbaix (potential vs. pH) diagram. Spin density distributions of the radical cations were examined regarding their relationship to the signature fine structure in the electron paramagnetic resonance spectra of the fluorinated derivatives of tryptophan. Electrostatic potential maps were calculated to provide a simple yet reliable means of evaluating charge distribution in the neutral and radical species. Results indicate that DFT mimicked the trends found in the Pourbaix diagram and gave insight into the properties of UAAs such as charge stabilization. Ultimately, a computationally-guided synthesis of an UAA, with its properties explicitly known, into the bacterial protein azurin could provide further insight into the PCET pathway.

Introduction

Proton-coupled electron transport (PCET) can take place over 35 Å yet the mechanism of PCET remains largely unexplored. It is important for biological functions such as DNA synthesis and repair and enzymes such as ribonucleotide reductase (RNR). The PCET pathway is aided by amino acid sidechains that facilitate the enzyme-catalyzed reactions.[3-5] Changes in protein conformation can mask PCET reactions and further hinder scientists from determining the mechanisms that fuel PCET.[5-9] With unnatural amino acids (UAAs), we hope to better understand this pathway. The goal of this study is to computationally examine UAAs and their properties such as ionization potentials (IPs), spin densities, interaction in solvent, and electrostatics.

Monitoring and modifying amino acids in proteins have been key players in understanding PCET because they act as signals for proton or electron transfer. While tyrosine has been extensively studied over the past decade[1,10-12] to determine its role, tryptophan could provide further insight due to its role as a radical scavenger. Tryptophan is the precursor to biological chemicals such as serotonin yet it is the least abundant amino acid.[13] Tryptophan has also shown an ability to scavenge radicals to prevent the formation of oxidation species.[14] These properties allow tryptophan to act as a beacon for electron transportation in pathways such as PCET. Furthermore, by using derivatives of tryptophan, it allows the behavior of the mechanism to be monitored.[15] The properties of tryptophan derivatives in comparison to tryptophan and their incorporation into proteins, such as azurin, have not been extensively studied.

Methods

Structure Optimization

Molecular structures were created using the Spartan 2018 software. They were then optimized to their minimum energy geometric orientation via Gaussian Suite Programs '09 using a B3LYP density functional and a 6-31+G* basis set. All neutral structures were optimized first. The optimized neutral structure went on to be the beginning structure for the optimizations of the corresponding radical cations, which are the product of an electron transfer process. For ionic structures, like for the radical cations, the appropriate combination of charge and multiplicity were specified in the job control section of the calculation. Here, the second optimization calculation designed to simulate an electron transfer was a neutral species. The structure of the 5-hydroxyindole ring included calculations with and without the hydrogen of the hydroxyl group. The hydrogen was removed because of the ambient pH of the cell would be sufficiently basic to deprotonate the group.

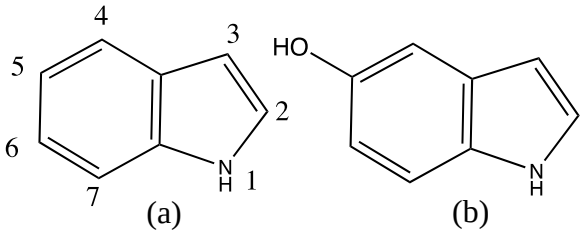

Figure 1: The (a) indole ring and (b) 5-hydroxyindole ring. The indole ring is labeled where substituents will be added.

The cartesian coordinates of optimized structures for the indole ring, 5-hydroxyindole, 4-fluoro-5-hydroxyindole, and 6-fluoro-5-hydroxyindole are given in the supplemental information.

More complete basis sets were used for comparison of the calculated spin densities. Such basis sets included the 6-31++G(d,p), CC-PVTZ, and 6-311+(3df,2p) sets, which add diffuse functions (improving the long-range description of the atom, important for anionic systems), polarization functions (functions of higher angular momentum in the atomic orbital descriptions), additional contractions (critical for flexibility of the electronic charge), and inclusion of effects due to the correlation of electronic motion.

Ionization Potentials

The ionization potential (IP) is the energy required to strip off an electron from a molecule. In order to calculate the IP, the optimized structures of the neutral molecule and its subsequent radical cation underwent frequency calculations. A frequency calculation involves evaluating the second derivative of the energy with respect to nuclear position. It serves a number of different purposes, including the determination of zero-point vibration and thermal corrections to the total energy as well as the enthalpic and entropic contributions. The ionization potentials were calculated from the sum of electronic and zero-point energies values from the frequency calculations by taking the difference between these energies for the ionized and neutral structures. IPs were evaluated for which varying levels of solvation were accounted: no solvent, approximated water solvent, explicit waters surrounding the structure, and then both solvent and explicit waters.

Electrostatic Maps

The electrostatic potential (ESP) maps provide an estimate of the predicted charge distribution across the molecular surface. The ESP maps were based on optimized structures and were rendered via the Gauss View visualization program module of the Gaussian 09 suite. In Gauss View, the ESP map is mapped onto the total density calculated with a fine grid.

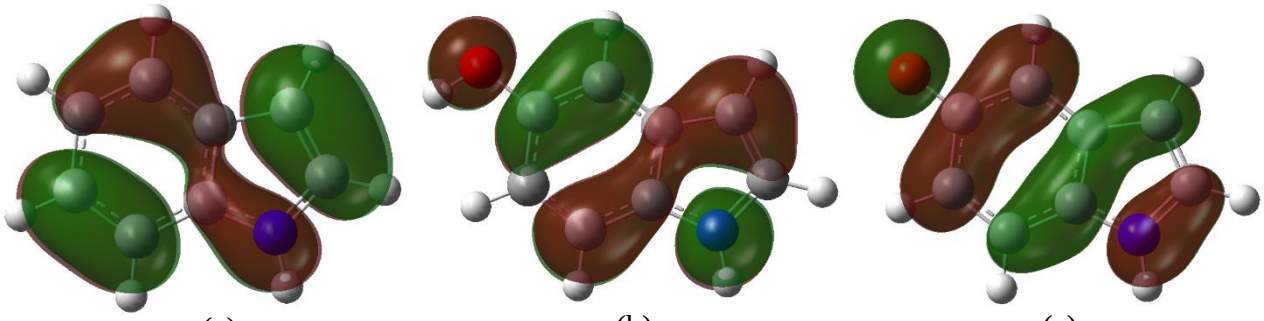

(a) (b) (c)

Figure 2: The HOMO for the (a) neutral indole ring, (b) neutral 5-hydroxyindol, and the (c) neutral radical deprotonated 5-hydroxyindole. The electron density indicates the ability of how the varied positions of the ring can donate/withdraw based on the location of the substituent.

Spin Densities

Spin densities show where the unpaired electron density resides in a molecule. The hydroxyl hydrogen was removed from the structure to mirror the neutral radical, deprotonated 5-hydroxyindole and its fluorinated derivatives used for EPR. After structures were optimized via Gaussian 09, they were exported to Spartan 18 and were subjected to further calculation with a B3LYP density functional and a 6-311+G(2df,2p) basis set. No solvent was used.

Results and Discussion

Ionization Potentials

Tryptophan was modified via hydroxylation with further substitutions such as amination, halogenation, and even more hydroxylation. This allowed extensive characterization on UAAs for tryptophan while establishing IP trends. IP values for a variety of tryptophan derivatives, and the well-characterized tyrosine, are shown in Appendix A. By varying the environment, the IP trends were established according to the aromatic ring substitutions trends. The IP values of the indole ring and its hydroxylated derivative, shown in Figure 1, were used as references in determining the effect of different substituents and their positions. The position of the hydroxyl group on the indole ring was kept constant, allowing the changing position of any other substituent's effect to be highlighted. The 4 position on the aromatic ring proved to donate more electrons into the ring and having a lowered IP value compared to the 6 position on the ring. The position of the substituent and its ability to contribute electrons to the ring is further supported by the highest occupied molecular orbital (HOMO), shown in Figure 2. The fourth position of

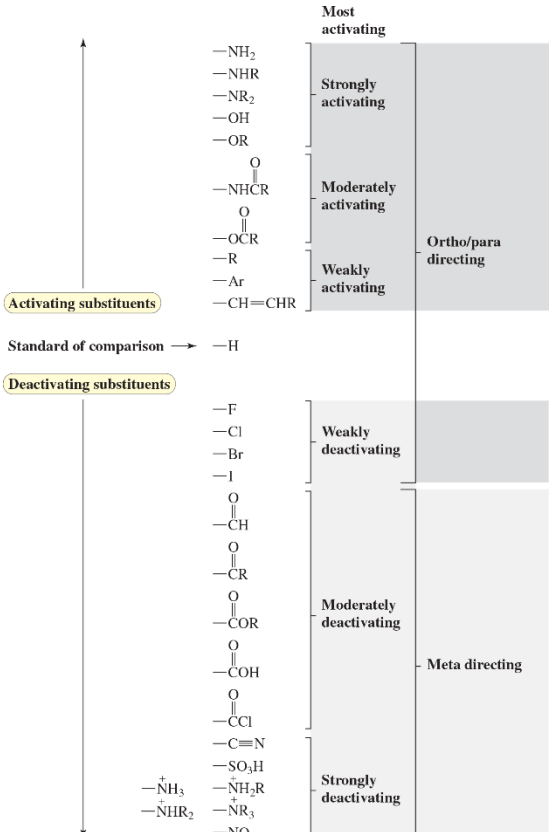

Figure 3: The effects of different substituents on aromatic rings. The substituents are activating the ring by donating electrons or deactivating by pulling electrons away from the ring.[16]

the indole ring has more π character relative to the sixth position. This is observed not only in the indole ring but as well as the 5-hydroxyindole ring that was the first UAA derivative of interest.

The substituent's identity impacted the IP value for the UAAs. As shown in Figure 3, amination and further hydroxylation were aromatic ring activators.[16] This resulted in further electron donation into the indole ring and lowered the IP value. It also demonstrates the substituents' behavior to primarily donate electrons despite its inductively withdrawing properties.

The fluorinated species was of interest because of its relevance in experimental incorporation. When tryptophan was halogenated (fluorine, chlorine, or bromine), an increase of IP was observed. Halogens deactivate the ring due to electronegativity. As electronegativity of the substituent increased, the ring became more deactivated and the IP value increased. Fluorine, being the more electronegative yet having the smallest radius, can maximize its orbital overlap and therefore attract more electrons. This effectively pulls electrons away from the ring and makes it harder to oxidize, resulting in an increased IP value. Table 1 demonstrates the fluorine's ability to decrease the IP of the indole ring while showing the effect of different positions on the ring has on the IP value.

Table 1: The comparison of 4-fluoro-5-hydroxyindole and 6-fluoro-5-hydroxyindole and their respective ionization potential values.

	No Solvent	Solvent	Explicit Waters
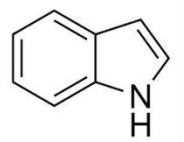	7.51	5.61	6.74
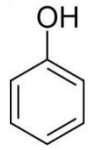	8.26	6.20	4.29
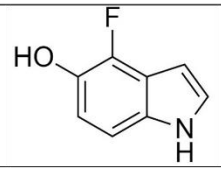	7.40	5.59	
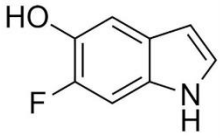	7.56	5.70	

Solution pK_a

The pH dependency of the oxidation potential for tyrosine and tryptophan was mimicked in the ionization potential trends (Table 1). Under no solvent and solvent conditions, the indole ring had a lower IP value than the phenol ring. A Pourbaix diagram, Figure 4, demonstrates this trend on the outer limits of the pH scale. However, native tyrosine (phenol ring) potential decreased lower than that of native tryptophan (indole ring) at a pH of approximately 4 – 12. When explicit waters were placed around the lone pairs on the hydroxyl group of the phenol or the amine on the indole ring,

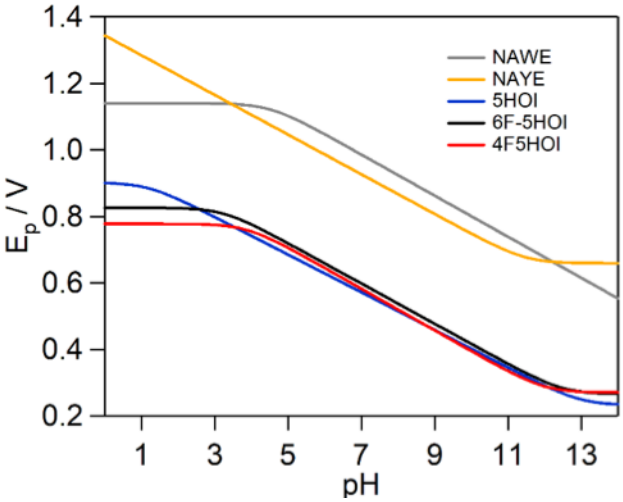

Figure 4: The Pourbaix diagram describing the pH dependence of the potentials for N-acetylated tyrosine and tryptophan as well as 5-hydroxyindole, 6-fluoro-5-hydroxyindole, and 4-fluoro-5-hydroxyindole. (Courtesy of Dr. Adam Offenbacher's lab.)

the trend represented in the Pourbaix diagram is mirrored. While pKa values are difficult to accurately measure via DFT, the addition of explicit waters to the system mimicked experimental conditions qualitatively.[17] This allowed the potential of the phenol ring to drop below that of the indole ring.

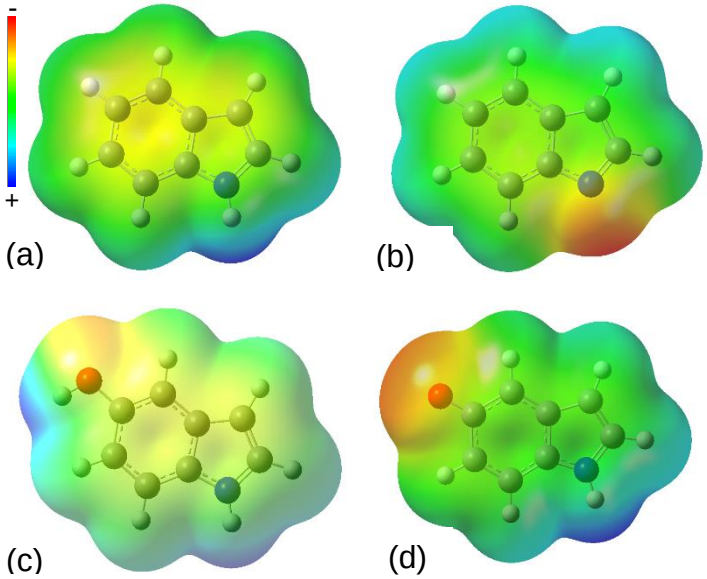

Figure 5: The electrostatic maps for the (a) indole ring (±0.06129), (b) deprotonated indole ring radical (±0.05151), (c) 5-hydroxyindole (±0.05175), and the (d) deprotonated 5-hydroxyindole radical (±0.07693).

Electrostatic Potential Maps

The electrostatic maps of the structures (Figure 5) demonstrate the charge distribution around the indole ring based on the substituents added. The increase in negative charge on the heterocyclic nitrogen once it is deprotonated reflects its ability to stabilize positive charges generated on other amino acids, such as histidine, during the PCET event.[18] Similarly, for 5-hydroxyindole, the hydroxyl group once deprotonated, provides a stronger stabilizing force at the oxygen for cations.

Spin Density

Visualization of the spin densities and the corresponding Mulliken charges (Figure 6) provides a clear rationale for the presence of a hyperfine signal in the EPR for the associated 4-fluorinated complex relative to the 6-fluorinated complex. The larger spin density at the C4 position couples to the nuclear spin of the adjacent fluorine to give rise to the signal seen in C of Figure 7.

This distinctive property of the fluorinated indole rings within tryptophan provides a measurable means of tracking the presence of the UAA in radical form and therefore affords a means to follow this feature of PCET the mechanism in azurin is investigated.

An analysis of the basis set dependence of the spin densities revealed that even-tempered balanced basis sets provided consistent results, in accord with previous.[19]

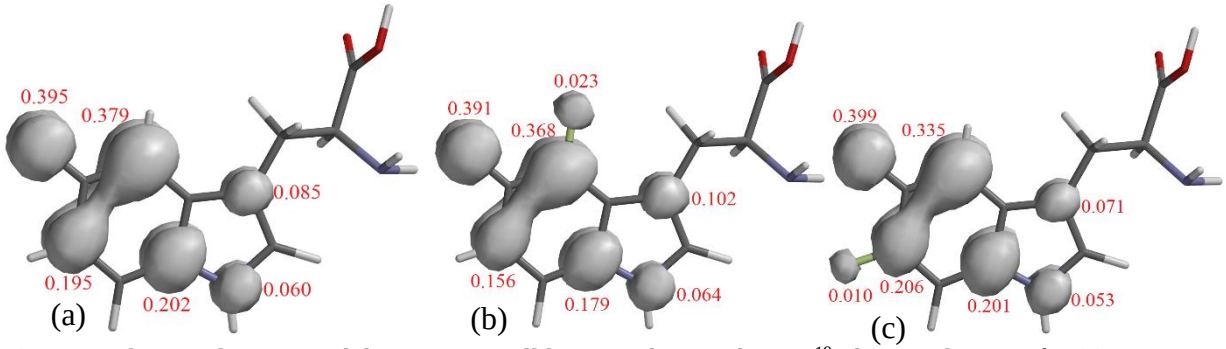

Figure 6*:* The spin densities and the positive Mulliken spin density charges.[19] The spin densities for (a) 5-hydroxytryptophan, (b) 4-fluoro-5-hydroxytryptophan, and (c) 6-fluoro-5-hydroxytryptophan.

Conclusion

Computational analysis of UAAs and their properties through DFT has provided further insight on how UAAs behave and their properties exploited in the study of the PCET mechanism. The UAA IP values demonstrate the importance of substituent identity on the indole ring. This contributed to the electron-donating or -withdrawing effects and impact the UAAs ability to lose an electron. Additionally, the location of the substituent proved to be essential in facilitating electron donation into the aromatic ring as demonstrated by the molecular orbitals. Analysis of ESP maps provides insight on the UAAs ability to stabilize cationic charges of surrounding amino acids or proteins. Finally, the spin densities of UAAs provided a clear rationale for how the 4-fluorinated complex can act as a radical tracker in the overall PCET process. DFT calculations have elucidated properties of UAAs seen in experimental data. Further DFT analysis could incorporate UAAs in a bacteria, azurin, as a next step in understanding PCET.

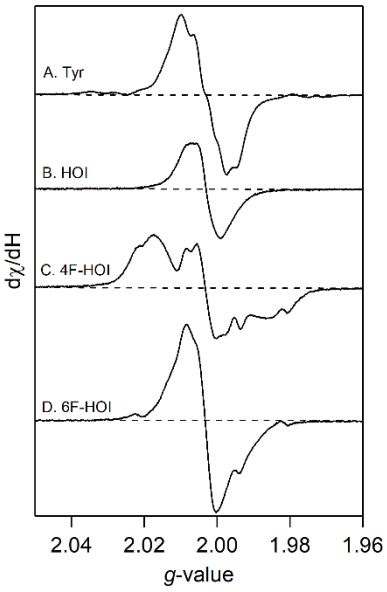

Figure 7: The electron paramagnetic resonance spectroscopy data (courtesy of Dr. Adam Offenbacher's lab).

References

1. Ravichandran, K. R.; Zong, A. B.; Taguchi, A. T.; Nocera, D. G.; Stubbe, J.; Tommos, C. Formal Reduction Potentials of Difluorotyrosine and Trifluorotyrosine Protein Residues: Defining the Thermodynamics of Multistep Radical Transfer. *J. Am. Chem. Soc.* **2017**, *139*, 2994-3004.

2. Minnihan, E. C.; Yokoyama, K.; Stubbe, J. Unnatural amino acids: better than the real things? *F1000 biology reports* **2009**, *1*, 88; 88-88.

3. Cukier, R. I.; Nocera, D. G. PROTON-COUPLED ELECTRON TRANSFER. *Annu. Rev. Phys. Chem.* **1998**, *49*, 337-369.

4. Huynh, M. H. V.; Meyer, T. J. Proton-Coupled Electron Transfer. *Chem. Rev.* **2007**, *107*, 5004-5064.

5. Hammes-Schiffer, S.; Stuchebrukhov, A. A. Theory of Coupled Electron and Proton Transfer Reactions. *Chem. Rev.* **2010**, *110*, 6939-6960.

6. Dempsey, J. L.; Winkler, J. R.; Gray, H. B. Proton-Coupled Electron Flow in Protein Redox Machines. *Chem. Rev.* **2010**, *110*, 7024-7039.

7. Migliore, A.; Polizzi, N. F.; Therien, M. J.; Beratan, D. N. Biochemistry and Theory of Proton-Coupled Electron Transfer. *Chem. Rev.* **2014**, *114*, 3381-3465.

8. Weinberg, D. R.; Gagliardi, C. J.; Hull, J. F.; Murphy, C. F.; Kent, C. A.; Westlake, B. C.; Paul, A.; Ess, D. H.; McCafferty, D. G.; Meyer, T. J. Proton-Coupled Electron Transfer. *Chem. Rev.* **2012**, *112*, 4016-4093.

9. Reece, S. Y.; Nocera, D. G. Proton-Coupled Electron Transfer in Biology: Results from Synergistic Studies in Natural and Model Systems. *Annu. Rev. Biochem.* **2009**, *78*, 673-699.

10. Seyedsayamdost, M. R.; Reece, S. Y.; Nocera, D. G.; Stubbe, J. Mono-, Di-, Tri-, and Tetra-Substituted Fluorotyrosines: New Probes for Enzymes That Use Tyrosyl Radicals in Catalysis. *J. Am. Chem. Soc.* **2006**, *128*, 1569-1579.

11. Range, K.; Ayala, I.; York, D.; Barry, B. A. Normal Modes of Redox-Active Tyrosine: Conformation Dependence and Comparison to Experiment. *J Phys Chem B* **2006**, *110*, 10970-10981.

12. Sjoberg, B. M.; Reichard, P.; Graslund, A.; Ehrenberg, A. The tyrosine free radical in ribonucleotide reductase from Escherichia coli. *J. Biol. Chem.* **1978**, *253*, 6863-6865.

13. Palego, L.; Betti, L.; Rossi, A.; Giannaccini, G. Tryptophan Biochemistry: Structural, Nutritional, Metabolic, and Medical Aspects in Humans. *Journal of amino acids* **2016**, *2016*, 8952520.

14. Weiss Günter; Diez-Ruiz Antonio; Christian, M.; Igor, T.; Dietmar, F. Tryptophan Metabolites as Scavengers of Reactive Oxygen and Chlorine Species. *Pteridines* **2013**, *13*, 140.

15. Lee, K. J.; Kang, D.; Park, H. Site-Specific Labeling of Proteins Using Unnatural Amino Acids. *Mol. Cells* **2019**, *42*, 386-396.

16. Bruice, P. Y. The Effects of Substituents on Reactivity. In *Organic Chemistry*; Zalesky, J., Ed.; Pearson: 2016; pp 886-889.

17. Thapa, B.; Schlegel, H. B. Density Functional Theory Calculation of pKa's of Thiols in Aqueous Solution Using Explicit Water Molecules and the Polarizable Continuum Model. *J Phys Chem A* **2016**, *120*, 5726-5735.

18. Sibert, R.; Josowicz, M.; Porcelli, F.; Veglia, G.; Range, K.; Barry, B. A. Proton-Coupled Electron Transfer in a Biomimetic Peptide as a Model of Enzyme Regulatory Mechanisms. *J. Am. Chem. Soc.* **2007**, *129*, 4393-4400.

19. Ayala, I.; Range, K.; York, D.; Barry, B. A. Spectroscopic Properties of Tyrosyl Radicals in Dipeptides. *J. Am. Chem. Soc.* **2002**, *124*, 5496-5505.